

# On-Chip Metamaterial Enabled Wavelength (De)Multiplexer

Yaotian Zhao, Jinlong Xiang, Yu He, Yuchen Yin, An He, Yong Zhang, Zongyin Yang, Xuhan Guo,\* and Yikai Su

Wavelength-division multiplexing (WDM) technology can offer considerable parallelism for large-capacity data communications. While several configurations have been demonstrated to realize on-chip WDM systems, their practical applications might be hindered by large footprints or compromised performances. Recently, metamaterial-assisted silicon photonics is emerging for on-chip light manipulation by subwavelength-scale control of optical wavefronts. They can reach more compact footprints and broadband functionalities beyond the classical waveguide-based architectures. Herein, wavelength (de)multiplexers are experimentally demonstrated in the subwavelength-structured metamaterials regime with highly compact footprints. Two-dimensional metamaterials composed of quasi-periodic dielectric perturbation arrays patterned on a multimode waveguide are proposed to stimulate multiple high-order waveguide modes at different wavelengths, which are then coupled to different WDM channels by cascading mode (de)multiplexers. The four-channel wavelength (de)multiplexer is demonstrated in a box-like spectrum with a compact footprint of  $2.5 \times 250 \mu\text{m}^2$ , with the measured losses less than 2 dB and channel crosstalk less than  $-14.3$  dB. By varying the patterned metamaterial structures, the proposed devices also have the merits of flexible operating wavelengths and bandwidths. The concept features large scalability, compactness, and competitive performance, which can offer versatile on-chip light manipulation and significantly improve the integration density for various on-chip WDM optical systems.

communication capacity by utilizing multiple wavelengths to simultaneously carry independent signals.<sup>[1]</sup> Wavelength (de)multiplexers are the key components for WDM systems to (de)multiplex signals.<sup>[2]</sup> Over the past decades, numerous wavelength (de)multiplexers have been reported based on conventional waveguide structures, for example, wavelength (de)multiplexers based on arrayed-waveguide gratings (AWGs) have good fabrication tolerance with low crosstalk, while they usually suffer from non-flat tops, relatively high insertion losses (ILs) and large footprints.<sup>[3]</sup> Wavelength (de)multiplexers based on multimode-interference (MMI) have moderate ILs and bandwidths, while their transmission spectra are also usually non-flat.<sup>[4]</sup> Additionally, wavelength (de)multiplexers employing cascaded Mach-Zehnder interferometers (MZIs) perform well with low ILs, large bandwidths, and moderate flat tops, while their requirements for the phase shift and coupling ratios are usually rigid.<sup>[5]</sup> Besides, wavelength (de)multiplexers based on micro-ring resonators (MRRs) have ultra-compact footprints with low ILs, while their response spectra usually have non-flat tops with limited

## 1. Introduction

Wavelength-division multiplexing (WDM) technology is one of the most competitive and efficient solutions to enhance


bandwidths and free spectral ranges (FSRs).<sup>[6]</sup> Recently, Bragg grating filters have also been actively demonstrated for on-chip WDM systems. The designs of Bragg grating filter are largely grouped into two main categories, grating assisted contra-directional couplers (GACDCs),<sup>[7–9]</sup> and multimode waveguide Bragg grating (MBG),<sup>[10–12]</sup> depending on whether the mode coupling operation occurs in the two separate waveguides or the same one. These filters have competitive performances with the merits of box-like spectral responses, low ILs, flexible bandwidths, and large FSRs. However, as they are operating in the Bragg reflection regime, there is an inherent trade-off between the operating bandwidth and the coupling length (see details in Section S1, Supporting Information), which significantly limits their miniaturization.

Dielectric metamaterials can offer a new perspective for silicon photonics with novel optical behaviors exceeding naturally available properties.<sup>[13]</sup> The maturity of silicon nanofabrication has ushered massive meta-structured waveguides

Y. Zhao, J. Xiang, Y. He, Y. Yin, A. He, Y. Zhang, X. Guo, Y. Su  
State Key Laboratory of Advanced Optical Communication Systems and Networks

Department of Electronic Engineering  
Shanghai Jiao Tong University  
Shanghai 200240, China  
E-mail: guoxuhan@sjtu.edu.cn

Z. Yang  
College of Information Science and Electronic Engineering  
State Key Laboratory of Modern Optical Instrumentation  
Zhejiang University  
Hangzhou 310027, China

 The ORCID identification number(s) for the author(s) of this article can be found under <https://doi.org/10.1002/lpor.202200005>

DOI: 10.1002/lpor.202200005

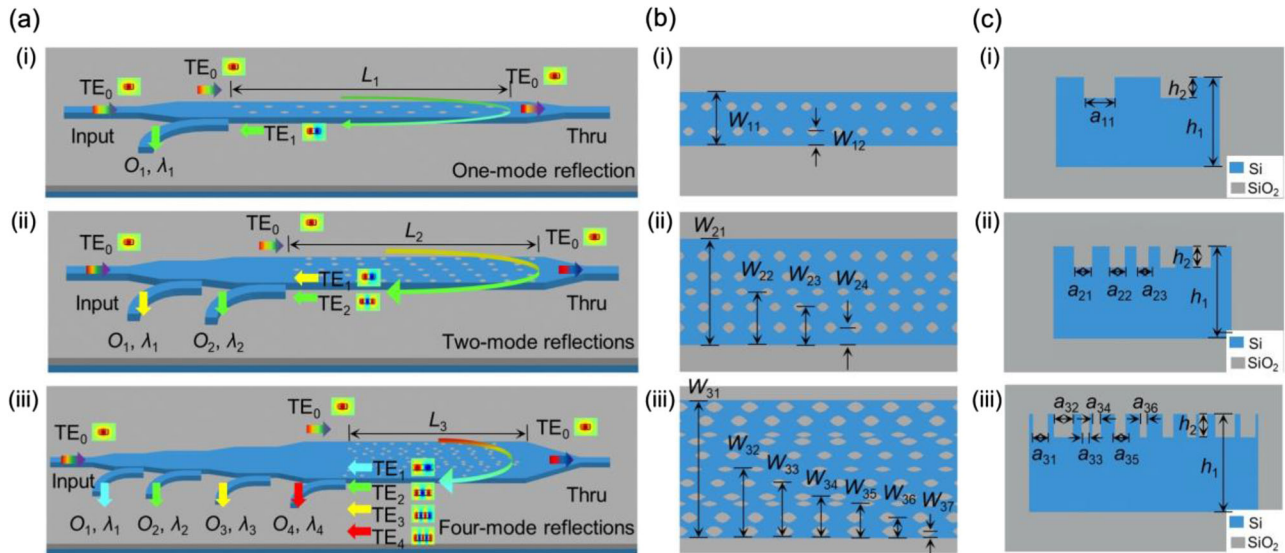


**Figure 1.** a) Schematics of the wavelength (de)multiplexers composed of a perturbed waveguide and a cascaded mode (de)multiplexer. b) Top and c) lateral views of the metamaterials composed of parallel dielectric hole arrays patterned on multimode waveguides. Panels i–iii) represent the metamaterial-enabled one-, two-, and four-channel wavelength (de)multiplexers.

available on a photonic chip, which provides efficient manipulation of guided electromagnetic waves.<sup>[14]</sup> Recently, the silicon metamaterial has been introduced to realize numerous high-performance nanophotonic devices, for example, bent multimode waveguides,<sup>[15]</sup> multimode crossings,<sup>[16]</sup> colorless couplers,<sup>[17]</sup> polarization-insensitive couplers,<sup>[18,19]</sup> mode-order converters,<sup>[20–23]</sup> and polarization beam splitters.<sup>[24]</sup>

In this paper, two-dimensional dielectric metamaterials are exploited to empower multi-channel WDM (de)multiplexers. The proposed metamaterial enabled wavelength (de)multiplexer is composed of parallel hole arrays patterned on a multimode waveguide with a designed phase-gradient along the propagation direction, where the input fundamental mode is reversely coupled to multiple high-order modes at user-defined wavelengths, which then are coupled out to different channels by cascading mode (de)multiplexers. As a proof of concept, we first demonstrate a metamaterial structure with two parallel hole arrays where the input TE<sub>0</sub> mode is coupled into a backward-propagating TE<sub>1</sub> mode at a specific wavelength channel. Then we demonstrate two and four wavelength channels respectively to verify the scalability, by increasing the parallel hole arrays in the multimode waveguides and enabling multiple high-order modes operations at designed channels. In this way, we give a new perspective of the metamaterial-enabled multi-channel wavelength (de)multiplexers. Compared to the conventional waveguide-based architectures, our proposed method provides a compact solution to multiply the channel numbers without increasing the coupling lengths. As a result, compact footprints of  $1.5 \times 95$ ,  $2 \times 150$ , and  $2.5 \times 250 \mu\text{m}^2$  for the one-, two-, and four-channel wavelength (de)multiplexers are demonstrated with competitive performances, especially for the box-like spectra, flexible operating wavelengths and bandwidths, which provide a viable route for versatile on-chip high-density WDM optical systems.

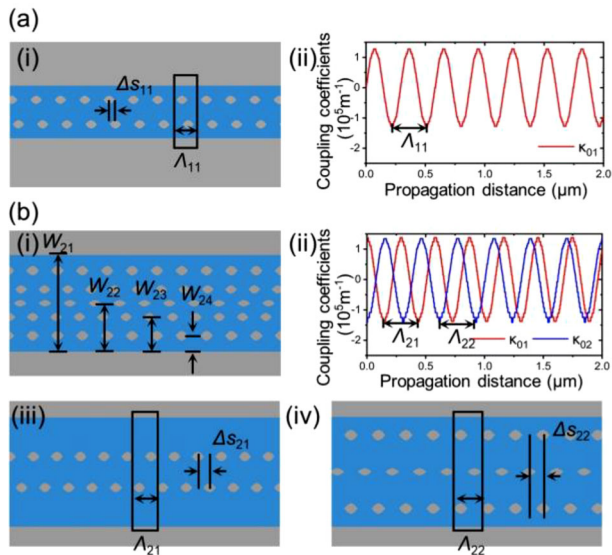
## 2. Design and Analysis

Figure 1 shows the schematics of our proposed (de)multiplexers as well as the top and lateral views of the metamaterials. The devices are designed based on a silicon-on-insulator (SOI) platform with a 220-nm-thick top silicon layer. Each structure consists of a multimode waveguide patterned with dielectric metamaterials as perturbations and asymmetric directional couplers (ADCs) as channel (de)multiplexers. The proposed metamaterials are designed to provide constructive interferences along the backward-propagation direction and proper phase-gradients along the propagation direction to excite specific modes. For the metamaterial structure shown in panel (i) of Figure 1a, the TE<sub>0</sub> mode launched from the input port is reversely coupled into the TE<sub>1</sub> mode at a designed wavelength, then coupled into the O<sub>1</sub> port by a TE<sub>1</sub>-selective mode (de)multiplexer. Likewise, for the dielectric metamaterial consisting of five parallel etching hole arrays on a wider waveguide shown in panel(ii), the input TE<sub>0</sub> mode is coupled into the backward-propagating TE<sub>1</sub> and TE<sub>2</sub> modes at different wavelengths, then coupled into O<sub>1</sub> and O<sub>2</sub> ports, respectively.

According to the classical coupled-mode theory (CMT) (see details in Section S1, Supporting Information), the effects of dielectric perturbation holes can be mathematically described by coupling coefficients  $\kappa$ , which can be expressed as Equation (1):<sup>[25]</sup>

$$\kappa_{mn}(z) = \kappa'_{mn} e^{-i\delta z} \quad (1)$$

where  $\kappa_{mn}$  is the coupling coefficient between the  $m$ th- and  $n$ th-order modes,  $\delta$  is dependent on the perturbation period  $\Lambda$  as  $\delta = 2\pi/\Lambda$ . When the parameter  $\delta$  compensates for the phase mismatch between the forward-propagating  $m$ th-order mode and backward-propagating  $n$ th-order mode, the mode coupling between these two modes will arise. This condition is also called



**Figure 2.** a) i) The top view and ii) corresponding calculated coupling coefficients of the metamaterial for one-mode reflection. b) i) The top view and ii) coupling coefficients for two-mode reflections, which consists of the hole arrays for iii) the TE<sub>1</sub> mode reflection, and iv) the TE<sub>2</sub> mode reflection.

the “phase-matching condition,” which can be mathematically expressed as Equation (2):<sup>[25]</sup>

$$\beta_m - (-|\beta_n|) - \delta = 0 \quad (2)$$

To put it simply, the perturbations that induce coupling coefficients with proper periods are required for mode conversions.

Then we introduce the designs of specific metamaterials according to the theoretical analysis by mapping the coupling coefficients to the dielectric metamaterial distributions. **Figure 2** shows the top views of the dielectric metamaterials and corresponding calculated coupling coefficients along a 2 μm-long section (detailed calculation method is shown in Section S1, Supporting Information). The legend  $\kappa_{ij}$  represents the coupling coefficient between the TE<sub>i</sub> mode and the TE<sub>j</sub> mode. For the one-mode reflection as shown in Figure 2a,  $\kappa_{01}$  is a periodic function of the propagation distance with the period  $\Lambda_{11}$ . When the dielectric etching holes induce periodic coupling coefficients that satisfy the phase-matching conditions as shown in Equation (2), the forward-propagating TE<sub>0</sub> mode will be completely coupled into the backward-propagating TE<sub>1</sub> mode. Besides, filters based on contra-directional couplings (CDC) usually suffer from strong sidelobes.<sup>[26]</sup> To suppress the sidelobes, lateral-shift apodization has been applied.<sup>[10,27]</sup> Specifically, longitudinal misalignment is introduced to the perturbations, and the superposition of the dielectric perturbations is modulated as a Gaussian function along the propagation distance  $z$ . The longitudinal shift  $\Delta s_{11}$  (see in Figure 2a) with an apodization index  $c_{11}$  is expressed as in Equation (3):

$$\Delta s_{11} = \frac{\Lambda_{11}}{2} \exp\left(-c_{11}(z - 0.5L_1)^2/L_1^2\right) \quad (3)$$

Note that the apodization is applied in a complementary manner to avoid phase errors for a rapid roll-off factor in the response spectrum.<sup>[28]</sup>

We now scale the concept to multiple mode reflections for multiple WDM channels. Here the multiple coupling coefficients are manipulated to be several periodic curves by the dielectric hole arrays, which can provide phase-matching conditions for multiple modes simultaneously.

Figure 2b shows the top view of the metamaterial for two high-order mode reflections and the corresponding mode coupling coefficients  $\kappa_{01}$  and  $\kappa_{02}$ . As we can see, the two coupling coefficients are two independent periodic functions with different periods  $\Lambda_{21}$  and  $\Lambda_{22}$ , which determine the operating wavelengths for the couplings of TE<sub>1</sub> and TE<sub>2</sub> modes respectively. Two groups of dielectric hole arrays are employed to construct the metamaterial: One is two parallel etching hole arrays with the period  $\Lambda_{21}$  for TE<sub>1</sub> mode reflection as shown in panel (iii), and another is the three parallel arrays with the period of  $\Lambda_{22}$  for TE<sub>2</sub> mode as shown in panel (iv). The TE<sub>1</sub> and TE<sub>2</sub> mode couplings can be manipulated independently by modifying these two kinds of metamaterial perturbations. Besides, a similar apodization method is applied, and the longitudinal misalignment  $\Delta s_{21}$  and  $\Delta s_{22}$  (see in Figure 2b) are separately modulated in complementary manners with apodization indices  $c_{21}$  and  $c_{22}$  as in Equation (4):

$$\begin{aligned} \Delta s_{21} &= \frac{\Lambda_{21}}{2} \exp\left(-c_{21}(z - 0.5L_2)^2/L_2^2\right), \\ \Delta s_{22} &= \frac{\Lambda_{22}}{2} \exp\left(-c_{22}(z - 0.5L_2)^2/L_2^2\right) \end{aligned} \quad (4)$$

The structures and corresponding calculated coupling coefficients for the metamaterial enabling four-mode reflections are shown in Section S2, Supporting Information.

The three-dimensional finite-difference time-domain (3D-FDTD) method is employed to simulate performances of the proposed metamaterial-enabled wavelength (de)multiplexers (supported by *Lumerical* FDTD solution).<sup>[29]</sup> The details of the simulation are shown in Section S3, Supporting Information. The operating wavelengths can be independently controlled by the periods of the grouped dielectric hole arrays, and the operating bandwidths can be manipulated by the sizes and depth of the holes (see details in Section S4, Supporting Information). Here we refer to the coarse-WDM (CWDM) wavelength grid in ITU-T G.694.2 for the designs of wavelength (de)multiplexers with a channel spacing of 20 nm. The device geometric parameters are summarized in **Table 1**. The thickness of top silicon layer  $h_1$  is 220 nm and the etching depth  $h_2$  is 40 nm to achieve suitable coupling strength. The waveguide widths are 0.85, 1.2, and 2 μm to support multiple high-order modes respectively. The top and bottom arcs of each single etching hole are defined as half of a sinusoidal function with a suitable amplitude and period for proper coupling coefficients.

**Figures 3** and **4** show the light propagation and reflection spectra for the proposed metamaterials. Figure 3a shows power distributions for one-mode reflection at different wavelengths. The input TE<sub>0</sub> mode couples to a backward-propagating TE<sub>1</sub> mode at 1550 nm where the phase-matching condition is satisfied, otherwise, it passes through directly (for example, at 1570 nm). **Figure 4a** shows its reflection spectrum has a flat top with ILs less

**Table 1.** Geometric parameters of the designed metamaterials.

Legend: Value [unit: $\mu\text{m}$ ]										
$L_1$ :60	$W_{11}$ :0.850	$W_{12}$ :0.225	$a_{11}$ :0.150	$h_1$ :0.220	$h_2$ :0.040	$\Lambda_{11}$ :0.314				
$L_2$ :60	$W_{21}$ :1.200	$W_{22}$ :0.600	$W_{23}$ :0.375	$W_{24}$ :0.200	$a_{21}$ :0.100	$a_{22}$ :0.125	$a_{23}$ :0.095	$\Lambda_{21}$ :0.292	$\Lambda_{22}$ :0.309	
$L_3$ :100	$W_{31}$ :2.000	$W_{32}$ :1.000	$W_{33}$ :0.800	$W_{34}$ :0.600	$W_{35}$ :0.500	$W_{36}$ :0.300	$W_{37}$ :0.100	$a_{31}$ :0.150	$a_{32}$ :0.170	
	$a_{33}$ :0.070	$a_{34}$ :0.130	$a_{35}$ :0.110	$a_{36}$ :0.07	$\Lambda_{31}$ :0.275	$\Lambda_{32}$ :0.287	$\Lambda_{33}$ :0.304	$\Lambda_{34}$ :0.330		

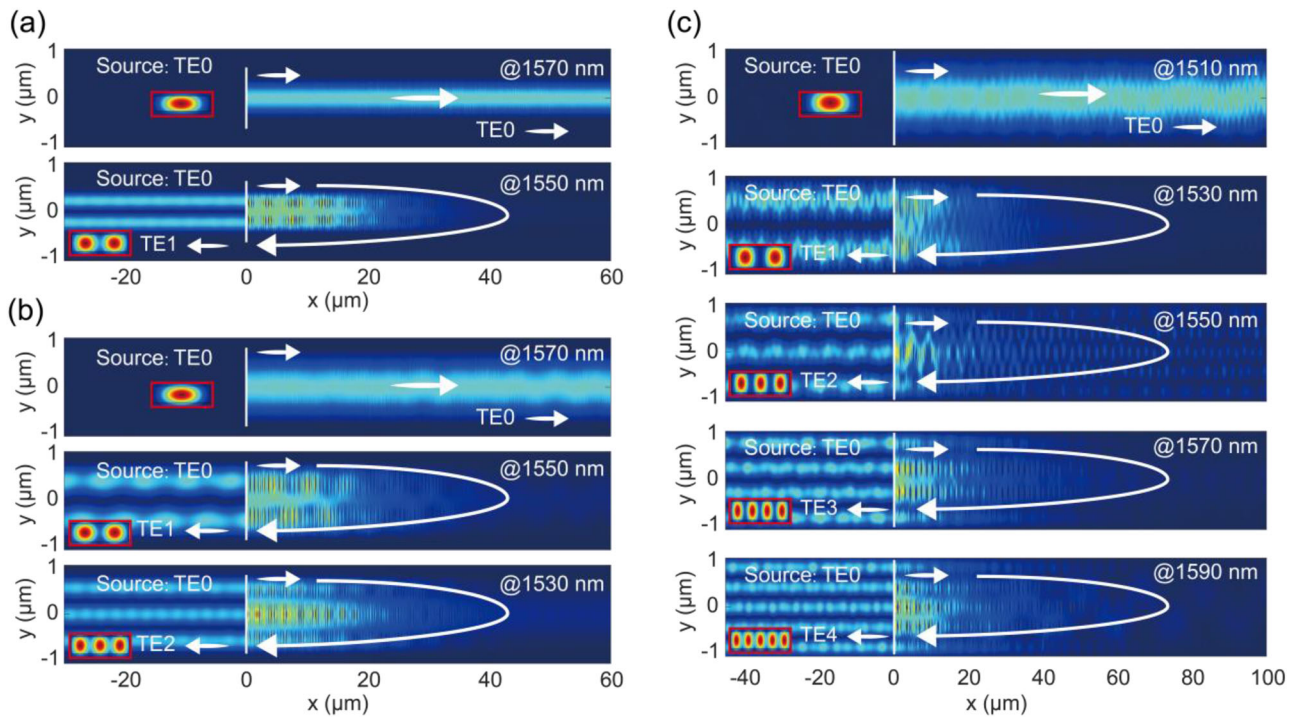


**Figure 3.** Simulated light propagation at different wavelengths of the metamaterial-enabled a) one-mode, b) two-mode, and c) four-mode reflections in the wavelength (de)multiplexers.

than  $-0.25$  dB, and the sidelobes suppress ratio (SLSR) is around 20.9 dB with the apodization index  $c_{11} = 15$ . Figures 3b and 4b describe the light propagation and reflection spectra for two high-order mode reflections. The input  $\text{TE}_0$  mode travels through at 1570 nm and couples to the  $\text{TE}_1$  and  $\text{TE}_2$  mode at 1550 and

1530 nm respectively, The ILs are less than 1 dB and the SLSRs are all above 19 dB with the apodization indices  $c_{21} = c_{22} = 10$ , and the channel crosstalk is less than  $-30$  dB. Similarly, Figures 3c and 4c show the light propagation for four-mode reflections, the input  $\text{TE}_0$  mode goes through at 1510 nm and is reflected into the

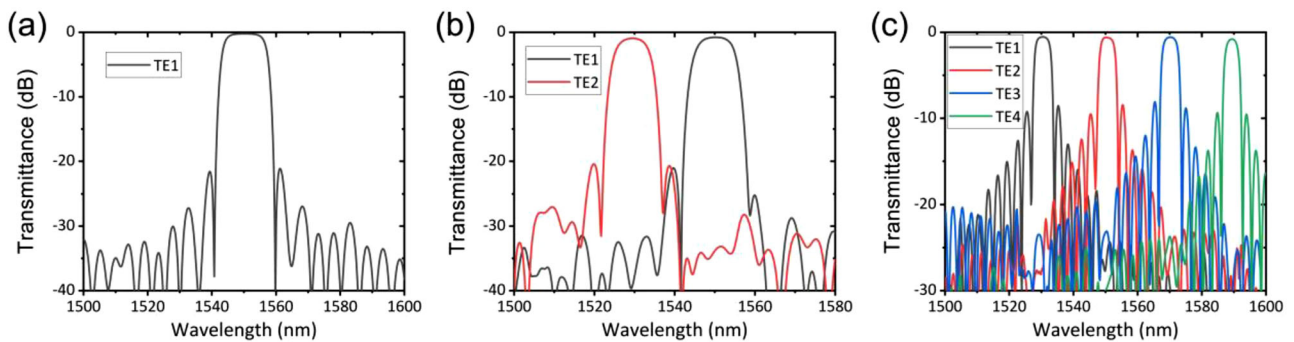


**Figure 4.** Simulated reflection spectra of the metamaterial-enabled a) one-mode, b) two-mode, and c) four-mode reflections in the wavelength (de)multiplexers.

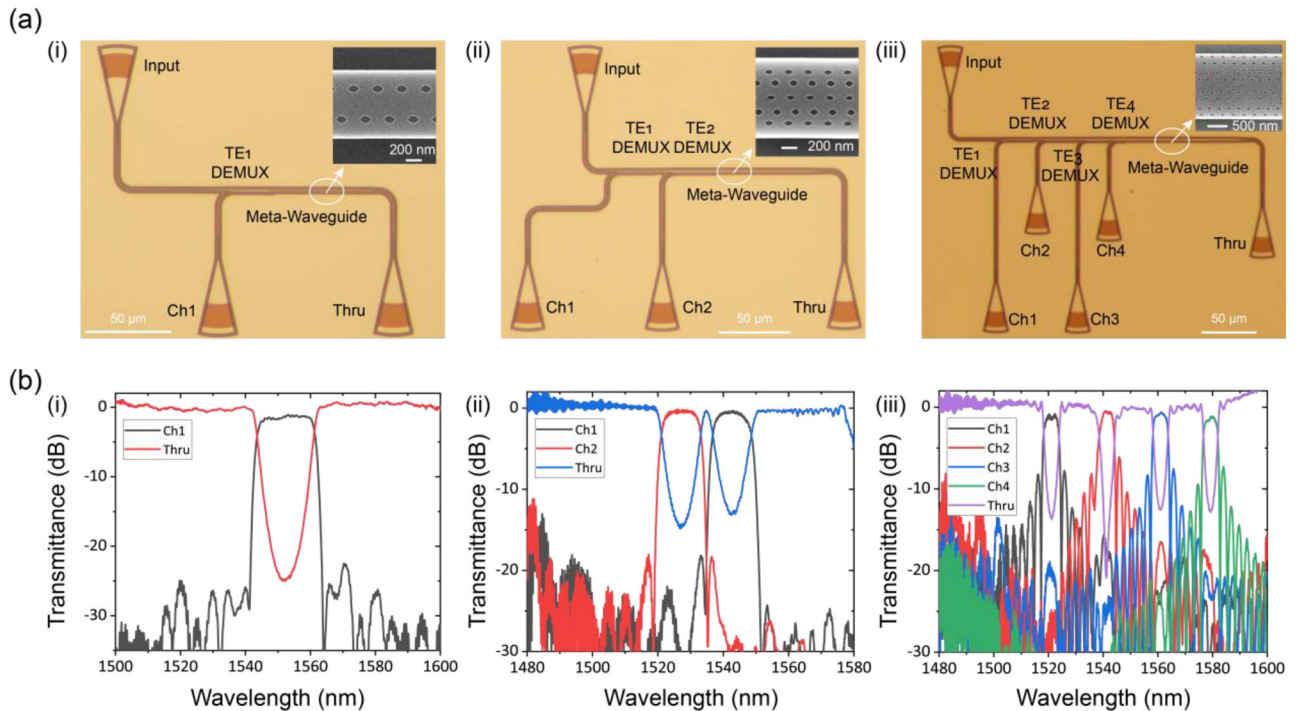


**Figure 5.** a) The optical microscope and scanning electron microscope (SEM) photos of the fabricated devices and b) the measured responses at different ports. Panels i–iii) represent the metamaterial-enabled one-, two-, and four-channel wavelength (de)multiplexers.

$TE_1$ ,  $TE_2$ ,  $TE_3$ , and  $TE_4$  mode at 1530, 1550, 1570, and 1590 nm, respectively. The reflection spectra have low ILs less than  $-0.8$  dB with channel crosstalk less than  $-25$  dB.

### 3. Fabrication and Characterization

The proposed metamaterial-enabled wavelength (de)multiplexers are fabricated on a standard SOI platform with a 220 nm silicon top layer. These structures are patterned employing e-beam lithography (EBL, Vistec EBPg-5200) and inductively coupled plasma (ICP) etching, covered with 1- $\mu$ m thick silicon dioxide employing inductively coupled plasma chemical vapor deposition (ICPCVD). An optical power meter (Santec, MPM210) and a tunable laser (Santec, TSL770) are used to characterize the device. Grating couplers (GC) are utilized to couple light between fibers and silicon waveguides. The cascaded mode (de)multiplexers based on ADC structures are used to couple the backward-propagating modes to different waveguide channels. The fabrication and characterization details of the mode (de)multiplexers are shown in Section S5, Supporting Information.<sup>[30]</sup>

**Figure 5** shows the microscope photos of our fabricated devices and the measured spectra at different ports. The spectra are normalized by reference grating couplers fabricated on the same chip (The spectra before normalization is shown in Section S6, Supporting Information for a check). Panel (i) of Figure 5a shows the structures of metamaterial-enabled one-channel wavelength (de)multiplexer. The  $TE_0$  mode injected from the input port is reflected and coupled into the Ch1 port centered at 1550 nm. The measured spectra at the Thru and Ch1 ports are shown in panel (i) of Figure 5b. The ILs are less than 1.5 dB,

which is larger than the simulated result (0.2 dB). This is attributed to the additional losses from cascaded ADCs-based mode (de)multiplexers. The measured SLSR is about 21 dB, and the 3-dB bandwidth is about 18.1 nm. Panel (ii) shows the case of two-channel wavelength (de)multiplexers. The input  $TE_0$  mode is coupled to  $TE_1$  and  $TE_2$  modes at 1520 and 1540 nm with a channel spacing of 20 nm. The bandwidths are about 13.2 nm with ILs less than 1.2 dB. The channel crosstalk is about  $-19.2$  dB with SLSR better than 16.5 dB. For the case of four-mode reflections shown in panel (iii), the input  $TE_0$  mode is reflected into the  $TE_1$ ,  $TE_2$ ,  $TE_3$ , and  $TE_4$  modes at 1520, 1540, 1560, and 1580 nm, then coupled into the Ch1, Ch2, Ch3, and Ch4 ports with according mode (de)multiplexers. The ILs are less than 2 dB and the channel crosstalks are less than  $-14.3$  dB. These experimental results largely agree with the simulations, except for the bandwidth and the central operating wavelengths, which could be attributed to the fabrication errors in the perturbation depths, waveguide widths as well as mode (de)multiplexers. These performances can be further improved by optimizing the fabrication processes. Moreover, the wavelength thermal tuning processes are also experimentally demonstrated in Section S7, Supporting Information to meet the more gridless and dynamic scenarios.

In **Table 2**, we summarize the main characteristics of state-of-the-art CWDM wavelength (de)multiplexers on the SOI platforms. It shows that our work has greatly reduced the device footprints without largely compromising the performances. Our experimental results realize the compact footprint of only  $2.5 \times 250 \mu\text{m}^2$  for four channels with bandwidths of 5.6 nm, which bypasses the footprint bottleneck limited by the tradeoff between the bandwidth and coupling length. The WDM channel numbers might be further scaled when more high-order modes

**Table 2.** Performance of some state-of-the-art CWDM demultiplexers.

Ref.	Structure	Channel number	Loss [dB]	Crosstalk [dB]	Footprint [ $\mu\text{m}^2$ ]	Bandwidth [nm]
[3]	AWG	4	$\approx 5$	$\approx -25$	$550 \times 3900$	$\approx 5$
[4]	MMI	4	$\approx 2$	$\approx -15$	$12 \times 1210$	$\approx 8.5$
[5]	MZI	4	$\approx 1$	$\approx -18$	$100 \times 300$	$\approx 16$
[7]	GACDC	4	$\approx 1$	$\approx -11$	$2 \times 600$	$\approx 12$
[10]	MBG	4	$\approx 1$	$\approx -18$	$40 \times 600$	$\approx 15$
This work	Metamaterial	1	1.5	–	$1.5 \times 95$	18.1
This work	Metamaterial	2	1.2	–19.2	$2 \times 150$	13.2
This work	Metamaterial	4	2	–14.3	$2.5 \times 250$	5.6

are involved, and it is possible for dielectric patterns to satisfy more phase-matching conditions. Indeed, this strategy requires lots of high-order mode demultiplexers, however, we note that the record high-order mode demultiplexers have been reported with 16 mode channels in our latest research,<sup>[31]</sup> which makes it promising to further utilize this route for more WDM channels. Besides, the metamaterial-enabled wavelength (de)multiplexers could also be arranged in a cascaded manner for more channels as shown in Section S8, Supporting Information. All the previous examples are demonstrated as wavelength demultiplexers, and these devices can also serve as wavelength multiplexers as shown in Section S9, Supporting Information.

## 4. Conclusion

We demonstrate novel multi-channel wavelength (de)multiplexers based on two-dimensional metamaterials with competitive performances and compact footprints. The coupling lengths of the perturbed waveguide are 60, 60, and 100  $\mu\text{m}$  for the one-, two-, and four-mode reflections, and the footprints of the wavelength (de)multiplexers are  $1.5 \times 95$ ,  $2 \times 150$ , and  $2.5 \times 250 \mu\text{m}^2$  with ILs less than 1.5, 1.2, and 2 dB, respectively. The operating bandwidth and wavelength can be flexibly designed by varying the metamaterial structures. The wavelength tunability has also been experimentally demonstrated by the thermal-tuning technique. Our proposed metamaterials now offer a new route for versatile on-chip spatial mode and wavelength manipulation in advance of conventional waveguide-based devices, which may enable novel functionalities in the development of hybrid wavelength- and mode-division multiplexing, nonlinear photonics, optical analog computing and beyond.

## Supporting Information

Supporting Information is available from the Wiley Online Library or from the author.

## Acknowledgements

This work was supported by National Key R&D Program of China (2019YFB2203104), Natural Science Foundation of China (NSFC) (#62175151 and #61835008), Natural Science Foundation of Shanghai (19ZR1475400), Open Project Program of Wuhan National Laboratory for

Optoelectronics (2018WNLOKF012). The authors also thank the Center for Advanced Electronic Materials and Devices (AEMD) of Shanghai Jiao Tong University (SJTU) and Tianjin H-chip Technology Group Corporation for their support in device fabrications.

## Conflict of Interest

The authors declare no conflict of interest.

## Data Availability Statement

The data that support the findings of this study are available in the Supporting Information of this article.

## Keywords

metamaterials, mode manipulation, multimode waveguides, silicon photonics, wavelength-division multiplexing

Received: January 3, 2022

Published online:

- [1] A. Liu, L. Liao, Y. Chetrit, J. Basak, H. Nguyen, D. Rubin, M. Paniccia, *IEEE J. Sel. Top. Quantum Electron.* **2009**, *16*, 23.
- [2] D. Liu, H. Xu, Y. Tan, Y. Shi, D. Dai, *Microw. Opt. Technol. Lett.* **2021**, *63*, 2252.
- [3] P. Pan, J. An, Y. Wang, J. Zhang, L. Wang, Y. Qi, Q. Han, X. Hu, *Opt. Laser Technol.* **2015**, *75*, 177.
- [4] Y. Hu, R. M. Jenkins, F. Y. Gardes, E. D. Finlayson, G. Z. Mashanovich, G. T. Reed, *Opt. Lett.* **2011**, *36*, 4488.
- [5] H. Xu, Y. Shi, *IEEE Photonics Technol. Lett.* **2017**, *30*, 169.
- [6] W. Bogaerts, P. de Heyn, T. van Vaerenbergh, K. de Vos, S. Kumar Selvaraja, T. Claes, P. Dumon, P. Bienstman, D. van Thourhout, R. Baets, *Laser Photonics Rev.* **2012**, *6*, 47.
- [7] W. Shi, H. Yun, C. Lin, M. Greenberg, X. Wang, Y. Wang, S. T. Fard, J. Flueckiger, N. A. F. Jaeger, L. Chrostowski, *Opt. Express* **2013**, *21*, 6733.
- [8] D. Charron, J. St-Yves, O. Jafari, S. LaRochelle, W. Shi, *Opt. Lett.* **2018**, *43*, 895.
- [9] K. Wang, Y. Yuan, X. Guo, Y. Zhang, A. He, Y. Su, *Front. Optoelectron.* **2021**, *14*, 374.
- [10] D. Liu, M. Zhang, Y. Shi, D. Dai, *IEEE Photonics Technol. Lett.* **2020**, *32*, 192.
- [11] D. Liu, H. Wu, D. Dai, *J. Lightwave Technol.* **2019**, *37*, 2217.

- [12] H. Qiu, J. Jiang, T. Hu, P. Yu, J. Yang, X. Jiang, H. Yu, *J. Lightwave Technol.* **2017**, *35*, 1705.
- [13] I. Staude, J. Schilling, *Nat. Photonics* **2017**, *11*, 274.
- [14] Y. Meng, Y. Chen, L. Lu, Y. Ding, A. Cusano, J. A. Fan, Q. Hu, K. Wang, Z. Xie, Z. Liu, Y. Yang, Q. Liu, M. Gong, Q. Xiao, S. Sun, M. Zhang, X. Yuan, X. Ni, *Light: Sci. Appl.* **2021**, *10*, 235.
- [15] H. Xu, Y. Shi, *Laser Photonics Rev.* **2018**, *12*, 1700240.
- [16] H. Xu, Y. Shi, *Laser Photonics Rev.* **2018**, *12*, 1800094.
- [17] R. Halir, P. Cheben, J. M. Luque-González, J. D. Sarmiento-Merenguel, J. H. Schmid, G. Wangüemert-Pérez, D. X. Xu, S. Wang, A. Ortega-Moñux, Í. Molina-Fernández, *Laser Photonics Rev.* **2016**, *10*, 1039.
- [18] H. Xu, Y. Shi, *Opt. Lett.* **2017**, *42*, 5202.
- [19] L. Liu, Q. Deng, Z. Zhou, *Opt. Lett.* **2016**, *41*, 1648.
- [20] Z. Li, M. Kim, C. Wang, Z. Han, S. Shrestha, A. C. Overvig, M. Lu, A. Stein, A. M. Agarwal, M. Lon, N. Yu, *Nat. Nanotechnol.* **2017**, *12*, 675.
- [21] H. Wang, Y. Zhang, Y. He, Q. Zhu, L. Sun, Y. Su, *Adv. Opt. Mater.* **2019**, *7*, 1801191.
- [22] D. Ohana, B. Desiatov, N. Mazurski, U. Levy, *Nano Lett.* **2016**, *16*, 7956.
- [23] Y. Zhao, X. Guo, Y. Zhang, J. Xiang, K. Wang, H. Wang, Y. Su, *Opt. Lett.* **2020**, *45*, 3797.
- [24] H. Xu, D. Dai, Y. Shi, *Laser Photonics Rev.* **2019**, *13*, 1800349.
- [25] C. Pollock, M. Lipson, *Integrated Photonics*, Springer, Boston, MA, USA **2003**.
- [26] H. Qiu, J. Jiang, P. Yu, T. Dai, J. Yang, H. Yu, X. Jiang, *Opt. Lett.* **2016**, *41*, 2450.
- [27] H. Qiu, L. Lin, P. Yu, T. Dai, X. Jiang, H. Yu, *J. Lightwave Technol.* **2019**, *37*, 5542.
- [28] H. Qiu, J. Niu, X. Liang, X. Shen, P. Yu, T. Dai, R. Cheng, *J. Lightwave Technol.* **2021**, *39*, 5896.
- [29] Lumeical, *Nanophotonic FDTD Simulation Software - Lumerical FDTD*, <https://www.lumerical.com/products/fdtd/> (accessed: December **2021**).
- [30] Y. He, Y. Zhang, Q. Zhu, S. An, R. Cao, X. Guo, C. Qiu, Y. Su, *J. Lightwave Technol.* **2018**, *36*, 5746.
- [31] Y. He, S. An, X. Li, Y. Huang, Y. Zhang, H. Chen, Y. Su, in *Optical Fiber Communication Conference*, Optical Society of America, San Diego **2021**, p. F3A.2.